*Journal of The Electrochemical Society*, **156** (1) A22-A26 (2009)
0013-4651/2008/156(1)/A22/5/$23.00 © The Electrochemical Society

# Pulsed-Laser-Deposited $Sn_4P_3$ Electrodes for Lithium-Ion Batteries

**Ji-Jin Wu and Zheng-Wen Fu**[*,z]

*Department of Chemistry and Laser Chemistry Institute, Shanghai Key Laboratory of Molecular Catalysts and Innovative Materials, Fudan University, Shanghai 200433, China*

$Sn_4P_3$ thin films have been successfully fabricated by reactive pulsed laser deposition for the first time and were investigated for their electrochemistry with lithium. The reversible discharge capacity of $Sn_4P_3$/Li cells cycled between 0 and 3.0 V was found to be about 906.2 mAh $g^{-1}$. By using ex situ X-ray diffraction, transmission electron microscopy, and selected-area electron diffraction measurements, both the classical alloying process and the phosphorization/reduction of nanosized Sn were revealed in the lithium electrochemical reaction of $Sn_4P_3$ film electrode. Large reversible capacity of $Sn_4P_3$ made it a potential anode material for future lithium-ion batteries.
 [DOI: 10.1149/1.3005960] 

Manuscript submitted June 23, 2008; revised manuscript received September 29, 2008. Published November 5, 2008.

The discovery that tin-based composites are of high theoretical capacity, which can be twice as much as carbon (372 mAh/g), made it one of the most impressive milestones in the field of Li-ion research.[1,2] Since then, much research has been devoted to tin-related materials, such as Sn alloy,[3-6] metal oxides of $SnO_2$, SnO and $Sn_2P_2O_7$,[7-9] $Sn_3N_4$,[10] SnSe,[11] $SnS_2$,[12] and $Sn_4P_3$.[13-15] Their higher capacities and relatively lower average working potentials indicate the possibility of using them as energy storage materials for the application and development of rechargeable lithium batteries. Among these tin-related materials, $Sn_4P_3$ is one of the most attractive lithium storage materials due to its two electroactive elements to lithium. Kim et al. reported that nanosized $Sn_4P_3$ prepared by mechanochemical synthesis retained a fairly large capacity of 370 mAh/g cycled in a limited voltage window, and a relatively large irreversible capacity can be due to the formation of $Li_3P$, which had been confirmed by X-ray absorption spectroscopic analysis and X-ray diffraction (XRD) data.[13] In order to improve the reversible capacity and cyclic efficiency, tin-rich $Sn_{4+\delta}P_3$ ($0 \leqslant \delta \leqslant 1$) was investigated as anode for lithium secondary batteries, and it was found that $Sn_5P_3$ exhibited a larger reversible capacity than that of $Sn_4P_3$.[14] Leon et al. investigated the electrochemical reaction mechanism of $Sn_4P_3$ by using magic angle spinning magnetic resonance and Mossbauer spectroscopy techniques. They found that reversibility was restricted to the formation of lithium–tin intermetallics and thus, the maximum allowed reversible capacity was limited.[15] In these studies, the reversible alloy–dealloy reaction of $Li_xSn$ after the initial reduction of tin phosphides to form Sn and $Li_3P$ was proposed when tin phosphides were cycled below 2.5 V in lithium cells. Recently, high reversible capacity of $SnP_{0.94}$ from structural reversibility by a lithium intercalation/deintercalation mechanism was reported without a phase transition from $SnP_{0.94}$ to metallic alloy $Li_xSn$.[16] Apparently, the intrinsic of the lithium electrochemical reaction with tin phosphides is complicated and data is still scarce. Further effort should be devoted to clarify the electrochemical reaction mechanism of tin phosphides with lithium.

It is well known that thin-film electrodes are free of additives and binders which are commonly used in powder-based electrodes and can be employed as an "ideal" system for fundamental studies, because they could yield greater insight into the intrinsic properties of the electrode materials. Pulsed laser deposition (PLD), as a simple and effective method for the fabrication of thin film, has experienced explosive growth in recent decades. However, there is no report on the thin-film fabrication and electrochemical properties of $Sn_4P_3$ prepared by PLD. In our previous works, we have used this method to investigate the electrochemical properties of thin-film electrodes of metal oxides,[17] nitrides,[18] selenides,[19] and fluorides.[20] Here, we report nanostructured thin film of $Sn_4P_3$ fabricated by PLD. The physical and electrochemical properties of $Sn_4P_3$ film electrodes are examined by galvanostatic cycling, cyclic voltammetry (CV), XRD, scanning electron microscopy (SEM), transmission electron microscopy (TEM), and ex situ selected area electron diffraction measurements (SAED). The purpose of this work is to clarify the electrochemical reaction mechanism of nanostructured thin film of $Sn_4P_3$ with lithium.

## Experimental

The apparatus used for PLD has been described elsewhere.[11] Experimental conditions for depositing thin films are described briefly as follows: A 355 nm laser beam, provided by the third harmonic frequency of a Q-switched Nd:yttrium aluminum garnet laser (Quanta-Ray GCR-150), was focused onto the surface of the target. The incident angle between the laser beam and the target surface normal was 45°. The laser energy intensity was 2 J $cm^{-2}$. The repetition rate and pulse width of the laser was 10 Hz and 10 ns, respectively. The targets were made from Sn and P powders (both pure 99.9%) mixed and ground in certain element molar ratios of Sn:P = 1:3 and then pressed to form a 1.3 cm diameter pellet as the ablated target. Excessive P in the target can compensate P loss due to its vacuum sublimation during laser ablation. The base pressure of the chamber was $10^{-2}$ Pa, and the ambient Ar gas pressure during deposition was kept at 5 Pa by a needle valve. The thin films were deposited on a stainless steel (SS) substrate, which was kept at 300°C. The distance between the target and the substrate was 4 cm. All the thin films were weighted by electrobalance (BP 211D, Sartorius, weight precision $\pm 0.01$ mg).

XRD patterns and the morphology of thin films were characterized by a Bruker D8 advance diffractometer equipped with Cu Kα radiation ($\lambda = 1.5406$ Å) and a scanning electron microscope (Philips XL30), respectively. TEM and SAED measurements were carried out by a 200 kV side-entry JEOL 2010 transmission electron microscope with energy-dispersive X-ray analyzers.

For the electrochemical measurements, the cells were constructed by using the as-deposited thin film as a working electrode and one lithium sheet as a counter electrode. The electrolyte consisted of 1 M $LiPF_6$ in a nonaqueous solution of ethylene carbonate and dimethyl carbonate (DMC) with a volume ratio of 1:1. The cells were assembled in an Ar-filled glove box. Galvanostatic cycling measurements were carried out at room temperature with a Land CT 2001A battery test system. The cells were cycled between 0 and 3.0 V vs $Li^+$/Li at a current density of 0.2 mA $cm^{-2}$. CV tests were performed with a scanning rate of 0.1 mV $s^{-1}$ between 0 and 3.0 V on a CHI660A electrochemical work station (CHI Instruments, TN).

In order to gain insight into the reaction mechanism of $Sn_4P_3$ with lithium, ex situ SEM, XRD, TEM, and SAED measurements were collected on the lithiated and delithiated $Sn_4P_3$ thin-film electrodes during the initial discharge and charge processes. The model

* Electrochemical Society Active Member.
z E-mail: zhengwen@sh163.net

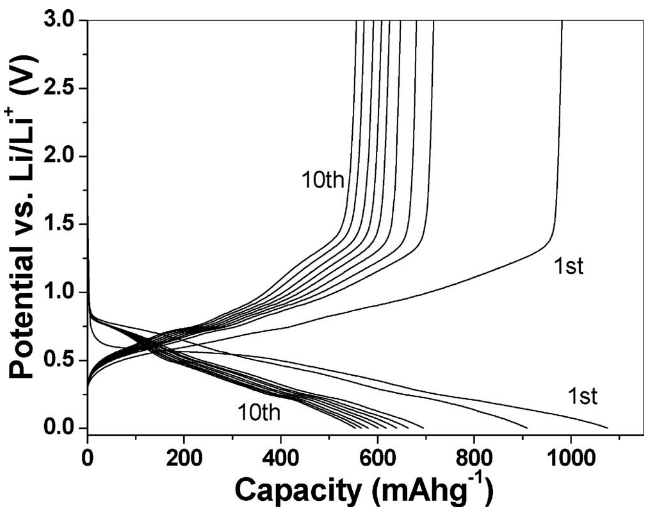


**Figure 1.** Galvanostatic curves of the as-deposited $Sn_4P_3$ thin-film electrode.

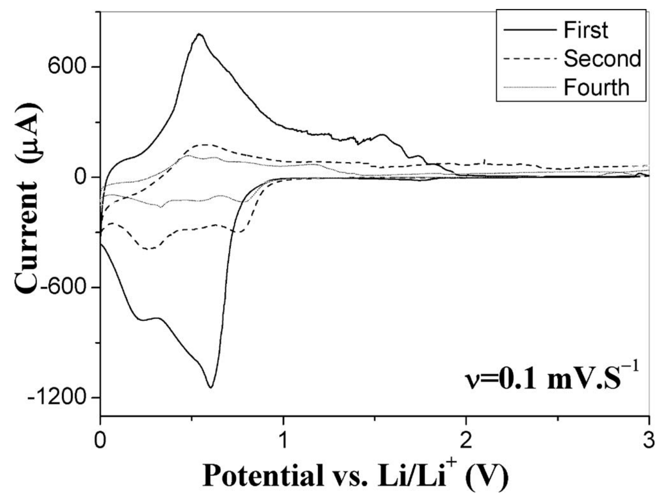


**Figure 2.** The first two cyclic voltammograms for the as-deposited $Sn_4P_3$ thin-film electrode.

cells were dismantled in an Ar-filled glove box and the electrodes were rinsed with anhydrous DMC to eliminate residual salts. For TEM and SAED measurements, the active materials were scratched from the SS substrate. The loose powders were then mixed with ethanol to prepare a slurry, out of which one drop was taken and deposited on a copper grid. To avoid exposure to oxygen or water, all the steps were done in a glove box protected by Ar and desiccant.

## Results and Discussion

Galvanostatic cycling was performed to examine the lithium electrochemical behavior of the as-deposited tin phosphide thin-film electrode. Voltage-capacity profiles of the tin phosphide cell cycled between 0 and 3.0 V under a current density of 0.2 mA cm$^{-2}$ are demonstrated in Fig. 1. The open-circuit voltage is around 1.55 V vs $Li^+$/Li. There are three discharge sloping plateaus in the first discharge curve appearing at around 0.70, 0.4, and 0.1 V, respectively. These discharge plateaus can be attributed to the electrochemical reaction of the as-deposited tin phosphide thin-film electrode with lithium. Correspondingly, three charge sloping plateaus in the first charge curve at around 0.7, 0.9, and 1.4 V are observed. In the subsequent cycles, the charge curve becomes more abrupt and moves to a higher value while the discharge plateaus decrease gradually, indicating that polarization has taken place during the discharge and charge cycles. The initial discharge capacity of the as-deposited tin phosphide thin film is found to be 1076 mAh g$^{-1}$. The second discharge process of the cell yields a reversible capacity of 906.2 mAh g$^{-1}$, which corresponds to 19 Li per $Sn_4P_3$. After 10 cycles, the discharge capacity is about 553 mAh g$^{-1}$. Such a large reversible capacity is superior to that of tin phosphide powder reported by previous works.[13-15] In addition, a high coulombic efficiency of about 92% is achieved in the first cycle, and the coulombic efficiency in the second cycle is found to be 79%. However, the coulombic efficiency in subsequent cycles is above 97%. This implies that the electrochemical process in the second cycle is different from the process in the first one. This may be related to the change of physical features of the sample after the first cycle.

Figure 2 shows the first, second, and the fourth cyclic voltammograms of the as-deposited tin phosphide thin-film electrode between 0 and 3.0 V measured at a scan rate of 0.1 mV s$^{-1}$. In the first cycle there are two cathodic current peaks appearing at 0.21 and 0.60 V, with two corresponding anodic peaks at 0.54 and 1.54 V. A couple of cathodic and anodic peaks at around 0.21 and 0.54 V could be attributed to the alloy and dealloy reaction between Li and Sn, respectively.[21] In the subsequent cycles, the position of this couple of peaks almost overlapped with that of the first cycle, demonstrating that a highly reversible reaction has taken place in the following cycles. However, the fact that both of them are fainter in the subsequent cycles illustrates great capacity loss. A substantial difference between the first and all subsequent cycles can be observed. The first reduction and oxidation process shows a cathodic peak at about 0.60 V and its corresponding anodic peaks at 1.53 V. When the electrode is completely activated, this pair of peaks disappears in subsequent cycles and instead, another two peaks emerge at 0.55 and 0.78 V, which are likely the counterparts of two anodic peaks at 0.62 and 1.16 V. This is in good agreement with the differential capacity plots of the $Sn_4P_3$ electrode,[14] in which the cathodic peak between 0.6 and 0.8 V should be assigned to the formation of various phases of $Li_xP$, and the formation of $Li_xP$ has been reported in the electrochemical reaction of P with Li in a black P/carbon composite electrode.[22] The cathodic peak below 0.5 V should be attributed to the formation of $Li_xSn$.

Figure 3 shows the ex situ XRD pattern of the tin phosphide thin-film electrodes at various states during the first discharge and charge process. Apart from three diffraction peaks appearing at $2\theta = 27.2$, 43.6, and 50.8° corresponding to the SS substrate (marked by asterisks) in the XRD pattern of the as-deposited tin phosphides (Fig. 3a), several XRD peaks at 26.40, 28.90, 30.33, 31.467, 44.50, 45.7, 54.49, and 56.53°, could be well assigned to the (012), (015), (0012), (107), (0114), (110), (0021), and (027) reflection of the $Sn_4P_3$ (JCPDS card no. 74-0255), indicating that the as-deposited tin phosphide thin film mainly consists of $Sn_4P_3$. After discharging to 0.5 V (Fig. 3b), these peaks of $Sn_4P_3$ become fainter and new peaks emerge at the same time. These new peaks at 30.64 and 32.01° can be ascribed to the (200) and (101) reflections, respectively, of the Sn (JCPDS card no. 04-0673). The peaks of metallic tin keep on growing with the appearance of three new peaks at the (200), (211), and (301) reflections of the Sn, while the signals of $Sn_4P_3$ are neglectable after the electrode is discharged to 0.3 V (Fig. 3c). These results suggest that the crystallized $Sn_4P_3$ decomposes with the formation of Sn at the same time. After discharging to 0 V (Fig. 3d), most of the existing tin has been consumed in a further reduction process. This may be due to the alloy reaction between Li and tin, which is in good accordance with CV curves. After charging to 0.9 V (Fig. 3e), most of the tin has been restored, which provides evidence regarding the dealloy reaction of Li–Sn alloy discussed above. When oxidation continues, the signals of tin decrease and neither tin nor tin phosphides are observed after charging to 3.0 V (Fig. 3f), indicating the tin may take part in the further oxidation reaction.

As shown in Fig. 3d and f, there are no other XRD peaks apart from faint tin peaks and SS substrate signals. However, it is unwise to conclude that there is no product other than tin after being dis-

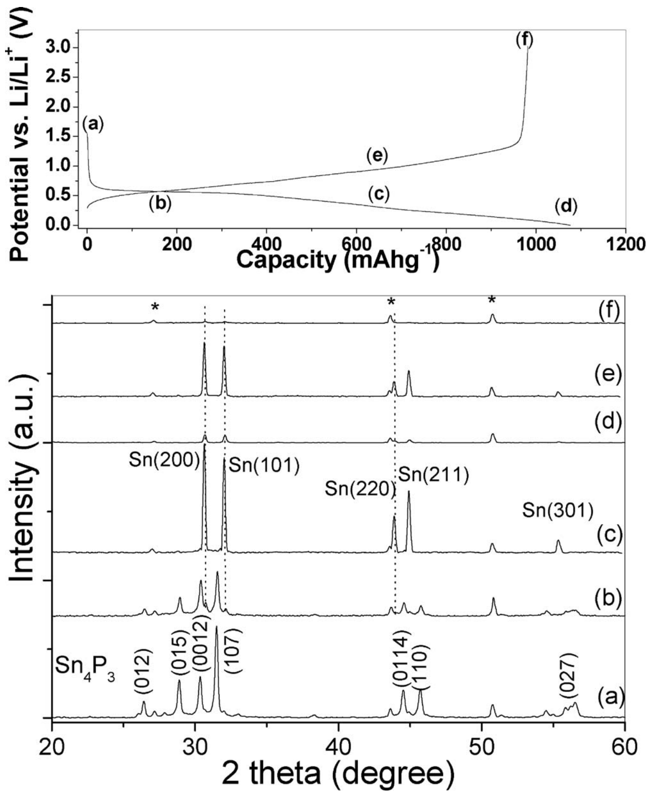


**Figure 3.** Ex situ XRD pattern of $Sn_4P_3$ thin-film electrodes at various states during the first discharge and charge process of the $Sn_4P_3$/Li cell (shown in the inset): (a) as-deposited, (b) after discharging to 0.5 V, (c) after discharging to 0.3 V, (d) after fully discharging to 0 V, (e) after charging to 0.9 V, and (f) after charging to 3.0 V. The peaks marked with an asterisk correspond to stainless steel substrate.

charged to 0 V, and few substances exist after charging to 3.0 V. Low crystallinity or crystallized but highly dispersed particles can also render themselves X-ray amorphous. To identify the modification occurring in the electrode after cycling, SAED and TEM studies were carried out to investigate the structure and composition of the fully discharged film and the fully charged electrode. For thin-film electrode after discharging to 0 V, particles of the product were found to be in the nanometer ranges in the TEM images shown in Fig. 4a. The average distance between the lattices of these crystallized particles is about 2.78 nm, which is close to the d-spacing of the (101) reflection of Sn. The SAED pattern in the region shows several clear rings made up of discrete spots (Fig. 4b). All d-spacings derived from the SAED pattern are shown in Table I. These rings could be unambiguously indexed to Sn, $Li_3P$ (JCPDS card no. 65-3512), and $Li_5Sn_2$ (JCPDS card no. 65-2121). Combined with the ex situ XRD results (Fig. 3), it is clear that $Li_3P$ is formed with the decomposition of $Sn_4P_3$, and $Li_5Sn_2$ is formed by lithiation of tin during the discharging process. The absence of $Li_5Sn_2$ or $Li_3P$ in Fig. 3d may be due to the sizes of these particles being less than X-ray coherence length (6 nm), which could not be identified by XRD. When the thin-film electrode is fully charged to 3.0 V, we could only see some faint stripes surrounded by ambiguous substances (Fig. 5a). The corresponding SAED pattern in this phase shown in Fig. 5b consists of three broad, weak rings, which also confirm the formation of a partially amorphous material. The reflections can be indexed to $Sn_4P_3$ (JCPDS card no. 74-0255). No trace of tin can be detected. This means that nanocrystalline $Sn_4P_3$ has been partially restored after charging to 3.0 V. Combined with the CV curve, it is easy to deduce that the cathodic peak around 1.54 V, which has not been revealed in previous references, corresponds to the formation of $Sn_4P_3$.

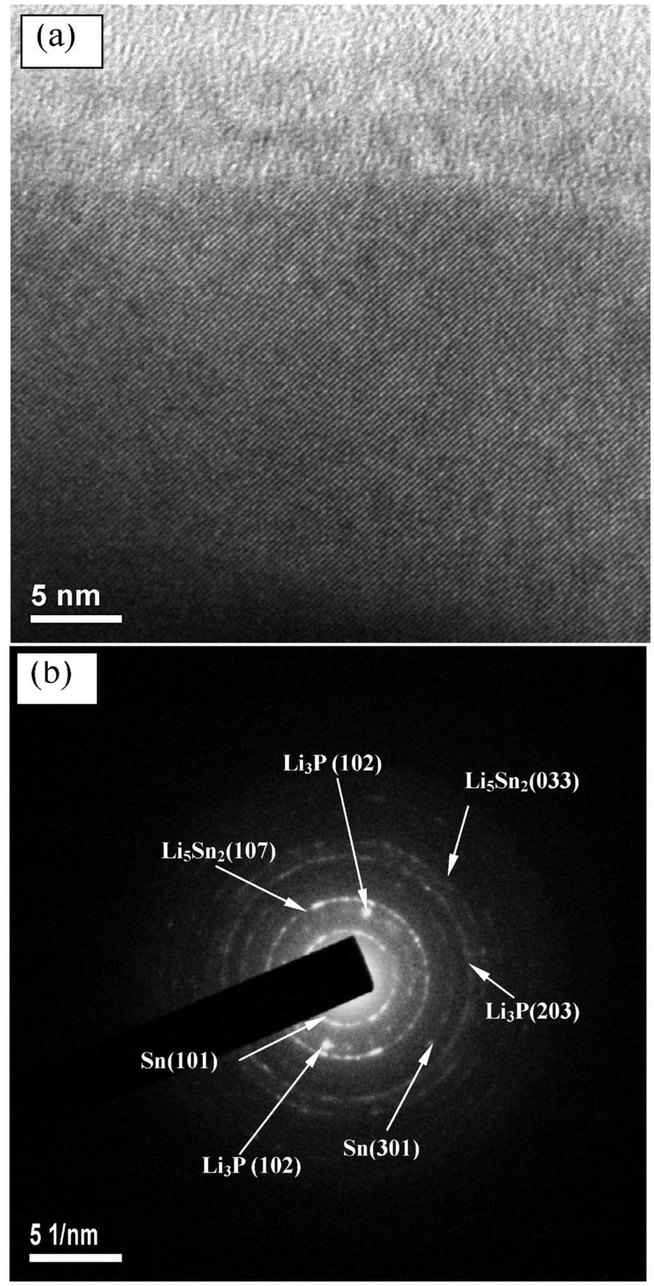


**Figure 4.** (a) TEM image and (b) corresponding SAED pattern of the lithiated $Sn_4P_3$ thin-film electrode after the first discharge to 0 V.

To determine the change in morphology of $Sn_4P_3$ induced by Li uptake/removal, SEM measurements were performed on as-deposited, lithiated, and delithiated $Sn_4P_3$ thin-film electrodes. Figure 6a-c shows SEM images of the as-deposited, lithiated, and delithiated $Sn_4P_3$ thin-film electrodes during the first cycle, respectively. As illustrated in Fig. 6a, particles of almost identical size (about 150 nm) and similar morphology can be observed. In comparing Fig. 6b with Fig. 6a, a clear difference in surface morphologies before and after lithiation of the thin film is apparent. Particles around 150 nm disappear. Instead, the surface becomes rougher and lavalike morphology emerges. The morphology change of the thin-film electrode after lithiation should be related to the initial discharge behaviors. After charging to 3.0 V for the first time, there are some agglomerates on the surface according to Fig. 6c. Combined with SAED results from Fig. 5, these particles are most likely $Sn_4P_3$ which is restored after the charging process.

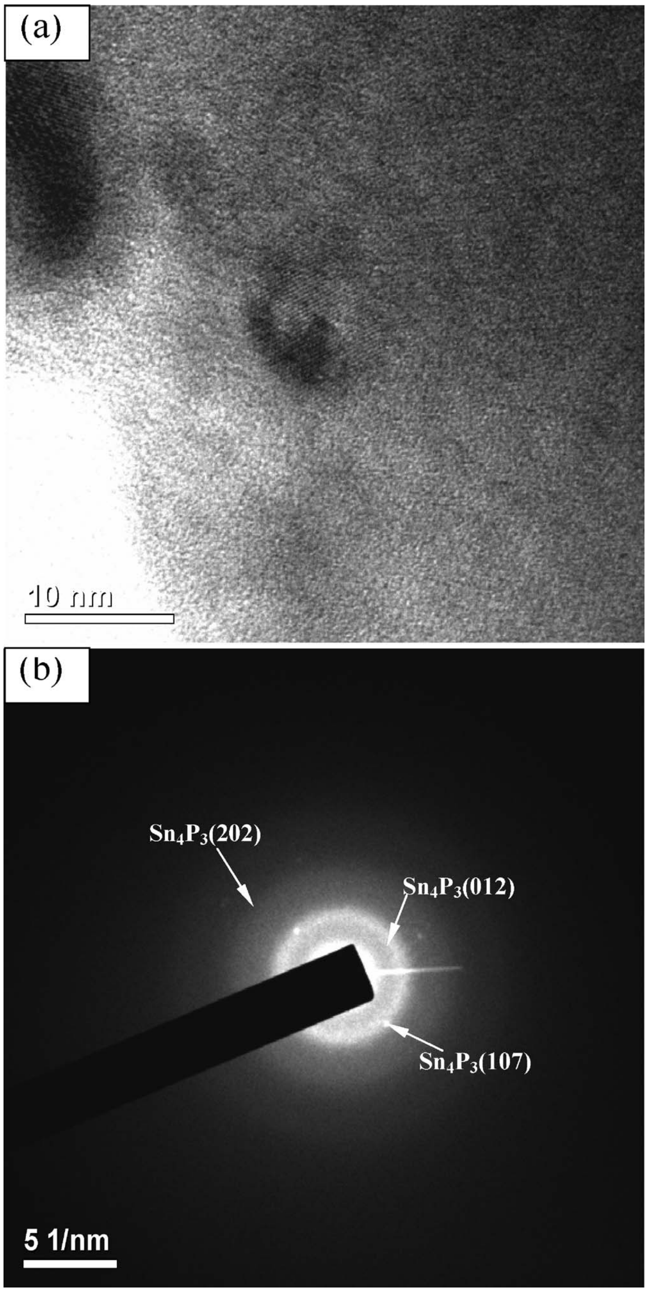


**Figure 5.** (a) TEM image and (b) corresponding SAED pattern of the delithiated $Sn_4P_3$ thin-film electrode after the first charging to 3.0 V.

According to the XRD and SAED data, the following electrochemical mechanism is proposed for $Sn_4P_3$ thin-film electrode with lithium:

Discharge process

$$Sn_4P_3 + 9Li \rightarrow 4Sn + 3Li_3P \ (1.55\text{–}0.5\ V) \quad [1]$$

$$2Sn + 5Li \rightarrow Li_5Sn_2 \ (0.5\text{–}0\ V) \quad [2]$$

Charge process

$$Li_5Sn_2 \rightarrow 2Sn + 5Li \ (0\text{–}0.9\ V) \quad [3]$$

$$4Sn + 3Li_3P \rightarrow Sn_4P_3 + 9Li \ (0.9\text{–}3.0\ V) \quad [4]$$

These steps during the discharge and charge processes are in accordance with CV curves as shown in Fig. 2. The first and second steps in the discharge process correspond to the cathodic peaks at 0.60 and 0.21 V, respectively, while the third and fourth steps in the charge processes correspond to the anodic peaks at 0.54 and 1.54 V, respectively. Although there is an irreversible structural change from the as-deposited crystalline $Sn_4P_3$ into nanocrystalline $Sn_4P_3$ the phosphorization/reduction reaction between nanocrystalline $Li_3P$ and Sn is reversible during the cycle, as shown in steps 1 and 4. A pair of reduction and oxidation peaks at 0.60 and 1.54 V, in the first CV curve can be assigned to the reduction and phosphorization of Sn. Apparently, Sn can drive the decomposition of $Li_3P$ with the

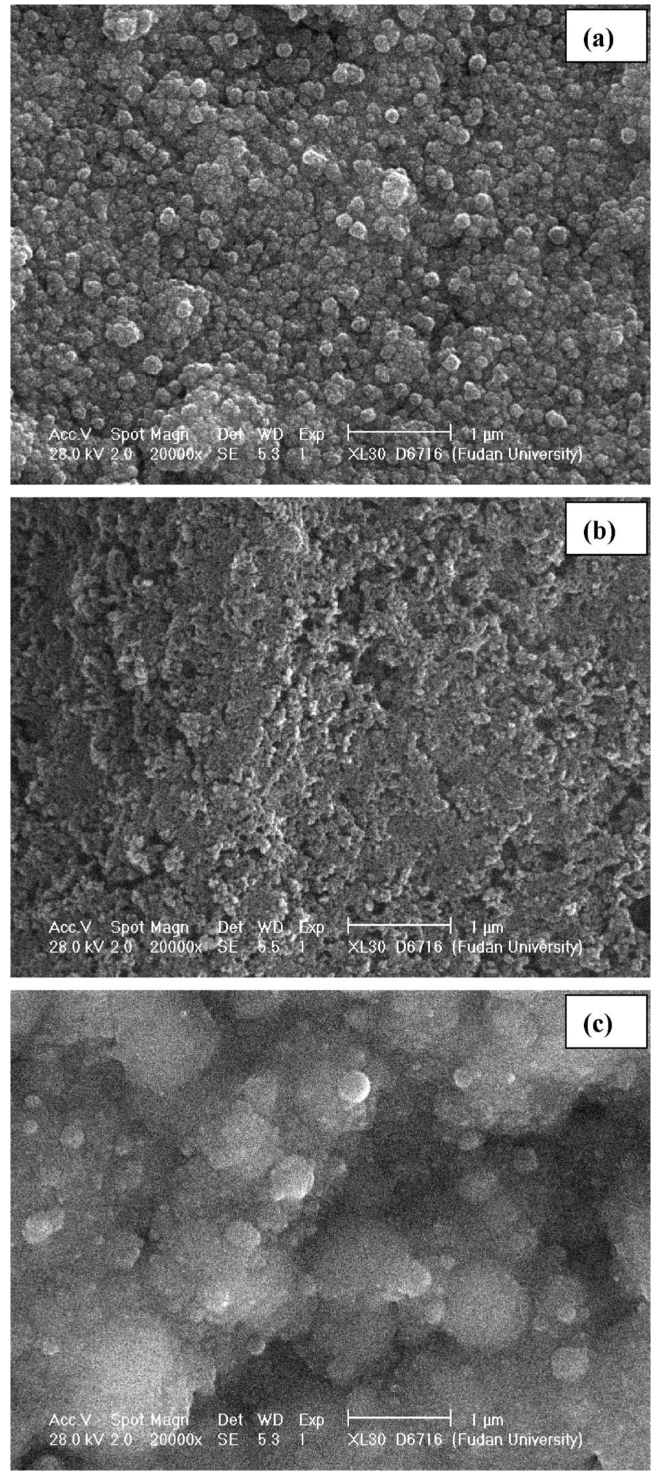


**Figure 6.** SEM images for $Sn_4P_3$ thin-film electrodes: (a) as-deposited, (b) after the first discharge to 0 V, and (c) after the first charge to 3.0 V.

formation of nanosized $Sn_4P_3$. In addition, the partially reversible alloying/dealloying reaction of Sn with lithium, as proposed in steps 2 and 3, indicates that Sn intermediate acts as a "stake holder" in lithium-consuming activities, in which $Li_2Sn_5$ and other amorphous Li–Sn intermetallic compounds in higher Li/Sn ratio may be formed.

It can be found that the electrochemical reaction mechanism of $Sn_4P_3$ thin film with lithium is different from that of bulk reported by Leon et al.,[15] in which the reversibility was restricted to the formation of lithium–tin intermetallics cycled between 0 and 2.5 V. Pralong et al. reported that metal cobalt from the decomposition of $CoP_3$ is an inactive center for reversible lithium intercalation/deintercalation processes between $Li_3P$ and LiP and acts as an "active spectator" without the formation of $CoP_3$.[23]

The original reason for the novel electrochemical mechanism of $Sn_4P_3$ thin-film electrode is rather complicated and involves multiple factors. First, thin-film electrode prepared by PLD is clean and compact, and as shown in Fig. 6a, it can avoid other impurities to suppress the reversible decomposition reaction of $Li_3P$ with Sn. Second, thin-film electrode could reduce the resistance of active material (the 280 nm thickness). In addition, thin-film electrode may provide more surface space to allow the volume change of the electrode due to Li insertion and reaction with active material, as shown in Fig. 6b and c, respectively.

Previous studies have shown that the reversible formation and decomposition of $Li_2O$ could be driven by nanosized Sn,[24] in which a Li-driven decomposition of $SnO_2$ into a composite matrix made of Sn dispersed into $Li_2O$; Sn particles are of nanosized dimensions and are well below the limit of detection in XRD measurement (less than 6 nm). Our present results provide another case. There are clear diffraction peaks from metal Sn(200) and Sn(101) in the lithiated thin films, as shown in Fig. 3e. The crystalline sizes of metallic Sn in the lithiated $Sn_4P_3$ thin films calculated by the Scherrer's formula[25] are found to be 25 nm from their XRD peak widths in Fig. 3e. Our results demonstrate that the well-crystalline metallic tin, with a crystal size of more than 6 nm, can also drive the decomposition of $Li_3P$.

According to the proposed mechanism, the nanosized $Li_3P$ and tin formed after the first discharge could have reactive activity. As a result, the reduction and phosphorization of metal tin could be observed and the thin-film electrode exhibited larger reversible capacity of 906.2 mAh $g^{-1}$ (corresponding to 19 Li per $Sn_4P_3$) in the galvanostatic cycling, more than the maximum capacity of Li-alloying with tin ($Li_{4.4}Sn$, corresponding to 17.6 Li per $Sn_4P_3$). The reversible conversion reaction of $Li_3P$ driven by metal tin into $Sn_4P_3$ could increase the reversible capacity remarkably based on the alloying reaction mechanism with lithium and make $Sn_4P_3$ a competitive anode material for lithium-ion batteries. However, the capacity fading of $Sn_4P_3$ thin-film electrode seems rather large. More effort should be devoted to reduce this fading and to make tin phosphides available in practical circumstances.

## Conclusions

$Sn_4P_3$ thin films have been successfully fabricated by reactive PLD. Galvanostatic cycling and CV measurements were used to examine the electrochemical behavior of $Sn_4P_3$/Li cells. A large reversible discharge capacity of 906.2 mAh $g^{-1}$ for a $Sn_4P_3$/Li cell was achieved. Two couples of reduction and oxidation peaks at 0.21 and 0.54 V and at 0.60 and 1.54 V in the first cycle were observed from the CV curves of a $Sn_4P_3$ thin-film electrode. By using ex situ XRD, TEM, and SAED measurements, both the alloying/dealloying processes and phosphorization/reduction processes of tin were revealed during the lithium electrochemical reaction of $Sn_4P_3$ thin-film electrode. Our results demonstrate that the reversible formation and decomposition of $Li_3P$ could be driven by metallic tin. The large reversible capacity of $Sn_4P_3$ thin-film electrode makes it a promising anode material for future lithium-ion batteries.

## Acknowledgment

This work was supported by the National Natural Science Foundation of China (project no. 20773031), 973 Projects (2007CB209702), and 863 Projects (2007AA03Z322).

*Fudan University assisted in meeting the publication costs of this article.*

## References

1. Y. Idota, M. Nishima, Y. Miyaki, T. Kubota, and T. Miyasaki, Eur. Pat. 0651450A1 (1995).
2. Y. Idota, T. Kubota, A. Matsufuji, Y. Maekawa, and T. Miyasaka, *Science*, **276**, 1395 (1997).
3. O. Mao, R. A. Dunlap, and J. R. Dahn, *J. Electrochem. Soc.*, **146**, 405 (1999).
4. H. Mukaibo, T. Sumi, T. Yokoshima, T. Momma, and T. Osaka, *Electrochem. Solid-State Lett.*, **6**, A218 (2003).
5. O. Mao, R. A. Dunlap, and J. R. Dahn, *J. Electrochem. Soc.*, **146**, 423 (1999).
6. K. D. Kepler, J. T. Vaughey, and M. M. Thackeray, *Electrochem. Solid-State Lett.*, **2**, 307 (1999).
7. I. A. Courtney and J. R. Dahn, *J. Electrochem. Soc.*, **144**, 2045 (1997).
8. W. F. Liu, X. J. Huang, Z. X. Wang, H. Li, and L. Q. Chen, *J. Electrochem. Soc.*, **145**, 59 (1998).
9. H. Li, X. Huang, and L. Chen, *Electrochem. Solid-State Lett.*, **1**, 241 (1998).
10. J. B. Bates, N. J. Dudney, B. Neudecker, A. Ueda, and C. D. Evans, *Solid State Ionics*, **135**, 33 (2000).
11. M. Z. Xue, J. Yao, S. C. Cheng, and Z. W. Fu, *J. Electrochem. Soc.*, **153**, A270 (2006).
12. T. Momma, N. Shiraishi, A. Yoshizawa, T. Osaka, A. Gedanken, J. Zhu, and L. Sominski, *J. Power Sources*, **97–98**, 198 (2001).
13. Y. U. Kim, C. K. Lee, H. J. Sohn, and T. Kang, *J. Electrochem. Soc.*, **151**, A933 (2004).
14. Y. U. Kim, S. I. Lee, C. K. Lee, and H. J. Sohn, *J. Power Sources*, **141**, 163 (2005).
15. B. Leon, J. I. Corredor, J. L. Tirado, and C. P. Vicente, *J. Electrochem. Soc.*, **153**, A1829 (2006).
16. Y. Kim, H. Hwang, C. S. Yoon, M. G. Kim, and J. Cho, *Adv. Mater. (Weinheim, Ger.)*, **19**, 92 (2007).
17. M. Z. Xue and Z. W. Fu, *Electrochem. Commun.*, **8**, 1250 (2006).
18. Z. W. Fu, Y. Wang, X. L. Yue, S. L. Zhao, and Q. Z. Qin, *J. Phys. Chem. B*, **108**, 2236 (2004).
19. M. Z. Xue, S. C. Chen, J. Yao, and Z. W. Fu, *Acta Phys. Chim. Sin.*, **22**, 383 (2006).
20. Z. W. Fu, C. L. Li, W. Y. Liu, Y. Wang, J. Ma, and Q. Z. Qin, *J. Electrochem. Soc.*, **152**, E50 (2005).
21. H. Li, X. J. Huang, and L. Q. Chen, *Solid State Ionics*, **123**, 189 (1999).
22. C. M. Park, and H. J. Sohn, *Adv. Mater. (Weinheim, Ger.)*, **19**, 2465 (2007).
23. V. Pralong, D. C. S. Souza, K. T. Leung, and L. F. Nazar, *Electrochem. Commun.*, **4**, 516 (2002).
24. M. Z. Xue and Z. W. Fu, *Electrochem. Solid-State Lett.*, **9**, A468 (2006).
25. B. D. Cullity, *Elements of X-Ray Diffraction*, 2nd ed., Addison-Wesley, Reading, MA (1978).